

# CURRENT APPLICATIONS OF X-RAY DIFFRACTION RESIDUAL STRESS MEASUREMENT

Paul S. Prevéy  
Lambda Research

## ABSTRACT

A brief theoretical development of x-ray diffraction residual stress measurement is presented emphasizing practical engineering applications of the plane-stress model, which requires no external standard. Determination of the full stress tensor is briefly described, and alternate mechanical, magnetic, and ultrasonic methods of residual stress measurement are compared.

Sources of error arising in practical application are described. Subsurface measurement is shown to be necessary to accurately determine the stress distributions produced by surface finishing such as machining, grinding, and shot peening, including corrections for penetration of the x-ray beam and layer removal.

Current applications of line broadening for the prediction of material property gradients such as yield strength in machined and shot peened surfaces, and hardness in steels are presented. The development of models for the prediction of thermal, cyclic, and overload residual stress relaxation are described.

X-RAY DIFFRACTION (XRD) STRESS MEASUREMENT can be a powerful tool for failure analysis or process development studies. Quantifying the residual stresses present in a component, which may either accelerate or arrest fatigue or stress corrosion cracking, is frequently crucial to understanding the cause of failure. Successful machining, grinding, shot peening, or heat treatment may hinge upon achieving not only the appropriate surface finish, dimensions, case depth or hardness, but also a residual stress distribution producing the longest component life. The engineer engaged in such studies can benefit by an understanding of the limitations and applications of XRD stress measurement. This paper presents a brief development of the theory and sources of error, and describes recent applications of material property prediction and residual stress relaxation.

Application of XRD stress measurement to practical engineering problems began in the early 1950's. The advent of x-ray diffractometers and the development of the plane-stress residual stress model allowed successful application to hardened steels (1,2). The development of commercial diffractometers and the work of the Fatigue Design and Evaluation Committee of the SAE (3) resulted in widespread application in the automotive and bearing industries in the 1960's. By the late 1970's XRD residual stress measurement was routinely applied in aerospace and nuclear applications involving fatigue and stress corrosion cracking of nickel and titanium alloys, as well as aluminum and steels. Today, measurements are routinely performed in ceramic, intermetallic, composite, and virtually any fine grained crystalline material. A variety of position sensitive detector instruments allow measurement in the field and on massive structures. The theoretical basis has been expanded to allow determination of the full stress tensor, with certain limitations.

Stress is an extrinsic property, and must be calculated from a directly measurable property such as strain, or force and area. The available methods of residual stress "measurement" may be classified into two groups: those that calculate stress from strain assuming linear elasticity, and those that monitor other nonlinear properties.

In x-ray and neutron diffraction methods, the strain is measured in the crystal lattice, and the residual stress producing the strain is calculated, assuming a linear elastic distortion of the crystal lattice. The mechanical linear-elastic methods (dissection techniques) monitor changes in strain caused by sectioning, and are limited by simplifying assumptions concerning the nature of the residual stress field and sample geometry. Center hole drilling is more widely applicable, but is limited to stresses less than nominally 60% of the yield strength (4). All mechanical methods are necessarily destructive, and cannot be directly checked by repeat measurement. All non-linear-elastic methods, such as ultrasonic and Barkhausen noise are subject to error from preferred

orientation, cold work, and grain size. All require stress-free reference samples, which are otherwise identical to the sample under investigation, and are generally not suitable for laboratory residual stress determination at their current state of development.

XRD residual stress measurement is applicable to fine grained crystalline materials that produce a diffraction peak of suitable intensity, and free of interference in the high back-reflection region for any orientation of the sample surface. Surface measurements are nondestructive. Both the macroscopic residual stresses and line broadening caused by microstresses and damage to the crystals can be determined independently.

Macroscopic stresses, or macrostresses, which extend over distances large relative to the grain size of the material, are the stresses of general interest in design and failure analysis. Macrostresses are tensor quantities, and are determined for a given location and direction by measuring the strain in that direction at a single point. Macrostresses produce uniform distortion of many crystals simultaneously, shifting the angular position of the diffraction peak selected for residual stress measurement.

Microscopic stresses, or microstresses, are treated as scalar properties of the material, related to the degree of cold working or hardness, and result from imperfections in the crystal lattice. Microstresses arise from variations in strain between the "crystallites" bounded by dislocation tangles within the grains, acting over distances less than the dimensions of the crystals. Microstresses vary from point to point within the crystals, producing a range of lattice spacing and broadening of the diffraction peak.

Because the elastic strain changes the mean lattice spacing, only elastic strains are measured by x-ray diffraction. When the elastic limit is exceeded, further strain results in dislocation motion, disruption of the crystal lattice, and an increase in line broadening. Although residual stresses are caused by nonuniform plastic deformation, all residual macrostresses remaining after deformation are necessarily elastic.

The residual stress determined using x-ray diffraction is the arithmetic average stress in a volume of material defined by the irradiated area, which may vary from square centimeters to less than a square millimeter, and the depth of penetration of the x-ray beam. The linear absorption coefficient of the material for the radiation used governs the depth of penetration. For the techniques commonly used for iron, nickel, and aluminum alloys, 50% of the radiation is diffracted from a layer less than 5  $\mu\text{m}$  deep. The shallow depth of penetration and small irradiated area allow measurement

of residual stress distributions with spatial and depth resolution exceeding all other methods.

## THEORY

A thorough development of the theory of x-ray diffraction residual stress measurement is beyond the scope of this paper. The interested reader is referred to the textbooks and general references (3,5,11,14). As in all diffraction methods, the lattice spacing is calculated from the diffraction angle,  $2\theta$ , and the known x-ray wavelength using Bragg's Law. The precision necessary for strain measurement in engineering materials can be achieved using diffraction peaks produced in the high back reflection region, where  $2\theta > 120$  deg. The macrostrain is determined from shifts typically less than one degree in the mean position of the diffraction peak. The microstresses and crystallite size reduction caused by plastic deformation are usually expressed simply in terms of diffraction peak angular width, which may range from less than 0.5 deg. for annealed material to over 10 deg. in a hardened steel.

**Plane-Stress Elastic Model.** Because the x-ray penetration is extremely shallow ( $< 10 \mu\text{m}$ ), a condition of plane-stress is assumed to exist in the diffracting surface layer. The stress distribution is then described by principal stresses  $\sigma_{11}$ , and  $\sigma_{22}$  in the plane of the surface, with no stress acting perpendicular to the free surface, shown in Figure 1. The normal component  $\sigma_{33}$  and the shear stresses  $\sigma_{13} = \sigma_{31}$  and  $\sigma_{23} = \sigma_{32}$  acting out of the plane of the sample surface are zero. A strain component perpendicular to the surface,  $\epsilon_{33}$ , exists as a result of the Poisson's ratio contractions caused by the two principal stresses.

$$\sigma_{33} = 0$$

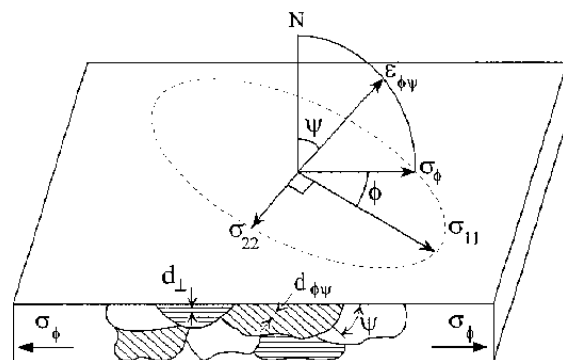


**Fig. 1** - Plane stress at a free surface showing the change in lattice spacing with tilt  $\psi$  for a uniaxial stress  $\sigma_\phi$  parallel to one edge.

The strain in the sample surface at an angle  $\phi$  from the principal stress  $\sigma_{11}$  is then given by:

$$\varepsilon_{\phi\psi} = \left( \frac{1+\nu}{E} \right) \sigma_{\phi} \sin^2 \psi - \left( \frac{\nu}{E} \right) (\sigma_{11} + \sigma_{22}) \quad (\text{Eq 1})$$

Equation 1 relates the surface stress  $\sigma_{\phi}$ , in any direction defined by the angle  $\phi$ , to the strain,  $\varepsilon_{\phi\psi}$ , in the direction  $(\phi, \psi)$  and the principal stresses in the surface. If  $d_{\phi\psi}$  is the spacing between the lattice planes measured in the direction defined by  $\phi$  and  $\psi$ , the strain can be expressed in terms of changes in the spacing of the crystal lattice:

$$\varepsilon_{\phi\psi} = \frac{\Delta d}{d_0} = \frac{d_{\phi\psi} - d_0}{d_0} \quad (\text{Eq 2})$$

where  $d_0$  is the stress-free lattice spacing. Substituting into Eq. 1 and solving for  $d_{\phi\psi}$  yields:

$$d_{\phi\psi} = \left[ \left( \frac{1+\nu}{E} \right)_{(hkl)} \sigma_{\phi} d_0 \right] \sin^2 \psi - \left( \frac{\nu}{E} \right)_{(hkl)} d_0 (\sigma_{11} + \sigma_{22}) + d_0 \quad (\text{Eq 3})$$

where the appropriate elastic constants  $(1+\nu)/E_{(hkl)}$  and  $(\nu/E)_{(hkl)}$  are now in the crystallographic direction normal to the  $(hkl)$  lattice planes in which the strain is measured. Because of elastic anisotropy, the elastic constants in the  $(hkl)$  direction commonly vary as much as 40% from the published mechanical values (5,6).

Equation 3 is the fundamental relationship between lattice spacing and the biaxial stresses in the surface of the sample. The lattice spacing  $d_{\phi\psi}$ , is a linear function of  $\sin^2 \psi$ . Figure 2 shows the variation of  $d(311)$  with  $\sin^2 \psi$ , for  $\psi$  ranging from 0 to 45° for shot peened 5056-O aluminum having a surface stress of -148 MPa (-21.5 ksi).

The intercept of the plot at  $\sin^2 \psi = 0$  equals the unstressed lattice spacing,  $d_0$ , minus the Poisson's ratio contraction caused by the sum of the principal stresses:

$$d_{\phi 0} = d_0 - \left( \frac{\nu}{E} \right)_{(hkl)} d_0 (\sigma_{11} + \sigma_{22}) = d_0 \left[ 1 - \left( \frac{\nu}{E} \right)_{(hkl)} (\sigma_{11} + \sigma_{22}) \right] \quad (\text{Eq 4})$$

The slope of the plot is:

$$\frac{\partial d_{\phi\psi}}{\partial \sin^2 \psi} = \left( \frac{1+\nu}{E} \right)_{(hkl)} \sigma_{\phi} d_0 \quad (\text{Eq 5})$$

which can be solved for the stress  $\sigma_{\phi}$ :

$$\sigma_{\phi} = \left( \frac{E}{1+\nu} \right)_{(hkl)} \frac{1}{d_0} \left( \frac{\partial d_{\phi\psi}}{\partial \sin^2 \psi} \right) \quad (\text{Eq 6})$$

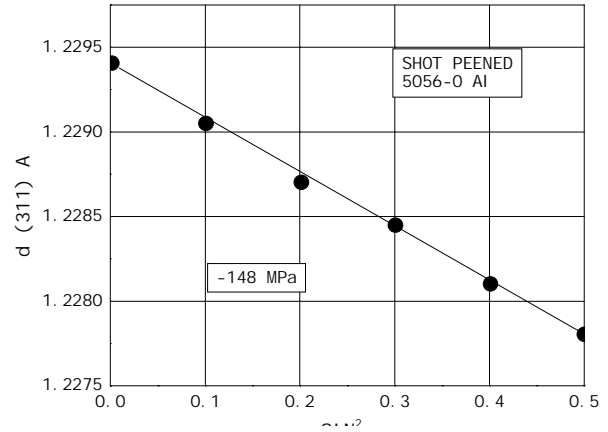


**Fig. 2** - Linear dependence of  $d(311)$  upon  $\sin^2 \psi$  for shot peened 5056-O aluminum. Ref. (14)

The x-ray elastic constants can be determined empirically (6), but the unstressed lattice spacing,  $d_0$ , is generally unknown. However, because  $E \gg (\sigma_{11} + \sigma_{22})$ , the value of  $d_{\phi 0}$  from Eq. 4 differs from  $d_0$  by not more than  $\pm 0.1\%$ , and  $\sigma_{\phi}$  may be approximated to this accuracy by substituting  $d_{\phi 0}$  for  $d_0$  in Eq. 6. The method then becomes a differential technique, and no stress-free reference standards are required to determine  $d_0$  for the plane-stress model. All of the common variations of x-ray diffraction residual stress measurement, the "single-angle", "two-angle", and " $\sin^2 \psi$ " techniques, assume plane-stress at the sample surface, and are based on the fundamental relationship between lattice spacing and stress given in Eq. 3.

**Stress Tensor Determination.** An expression for the lattice spacing can be formulated as a function of  $\phi$  and  $\psi$ , for the general case, assuming stresses exist normal to the surface<sup>(7)</sup>. Nonlinearities producing separation of the  $+\psi$  and  $-\psi$  data in the form of elliptical curvature of the  $d$ - $\sin^2 \psi$  plots termed " $\psi$  splitting" are occasionally observed at the surface of ground hardened steels, and are attributable to shear stresses acting normal to the surface<sup>(8)</sup>. Determination of the full stress tensor has been the focus of most academic research into XRD stress measurement over the last decade, and is necessary in all neutron diffraction applications because of the deep penetration into the sample.

In principle, the full stress tensor can be determined (7, 8). However, unlike the plane-stress model, the stress-free lattice spacing,  $d_0$ , must be known independently to the accuracy required for strain measurement (1 part in

$10^5$ ) in order to calculate the three normal stress components,  $\sigma_{11}$ ,  $\sigma_{22}$ , and  $\sigma_{33}$ . Errors in the normal stress components, which are of primary interest, are proportional to the difference between the value of  $d_0$  assumed and  $d_{\phi_0}$ . Large errors in both magnitude and sign of the three normal stress components can easily arise from errors in  $d_0$ . In most practical applications, such as the surfaces generated by machining, grinding, or hardening, the lattice spacing varies as a result of plastic deformation or heat treatment, precluding independent determination of the unstressed lattice spacing with sufficient precision (9-11). Further, other sources of nonlinearities in  $d\text{-sin}^2\psi$  plots such as subsurface stress gradients, instrument misalignment, and failure of the diffraction peak location method must first be eliminated (12,13). The full stress tensor method is therefore limited primarily to research applications.

## SOURCES OF ERROR

Because XRD residual stress determination requires precision in the measurement of the angular position of diffraction peak on the order of 1 part in  $10^5$ , many sources of error must be controlled. A thorough discussion of error is beyond the scope of this paper and have been addressed (3,5,11). The sources of error of primary importance in engineering applications may be placed in three categories: sample dependent errors, analytical errors, and instrumental errors.

Sample dependent errors may arise from an excessively coarse grain size, severe texture, or interference of the sample geometry with the x-ray beam. Both surface and subsurface stress gradients are common in machining and grinding, and may cause errors as high as 500 MPa, even altering the sign of the surface stress. Corrections can be made for penetration of the x-ray beam into the subsurface stress gradient using electropolishing to remove layers in fine increments on the order of 5-10  $\mu\text{m}$  (3,1).

Electropolishing for subsurface measurement will cause stress relaxation in the layers exposed. If the stresses in the layers removed are high and the rigidity of the sample is low, the relaxation can be on the order of hundreds of MPa. For simple geometries and stress fields, closed form solutions are available (15). Recently, finite element corrections have been applied to arbitrary geometries (16).

Analytical errors may arise from the validity of the stress model assumed, the use of inaccurate elastic constants, or the method of diffraction peak location. Diffraction peaks several degrees wide must be precisely located within 0.01 deg. Various methods have been developed,

but the fitting of Pearson VII functions to separate the  $K\alpha$  doublet and allow for peak defocusing caused by the change in  $\psi$  angle and line broadening as layers are removed in subsurface measurement is superior (12,13). X-ray elastic constants may be determined empirically to ASTM E1426 to an accuracy on the order of  $\pm 1\%$  in four-point bending (6).

Instrumental errors arise from the misalignment of the diffraction apparatus or displacement of the specimen. Sample displacement from the center of the goniometer is the primary instrumental error. Divergence of the x-ray beam and sample displacement can cause " $\psi$  splitting" which is indistinguishable in practice from the presence of shear stresses,  $\sigma_{13}$  and  $\sigma_{23}$ , acting out of the surface. ASTM E915 provides a simple procedure using a zero stress powder to verify the instrument alignment, except for the accuracy of the  $\psi$  rotation.

## SUBSURFACE MEASUREMENT

X-ray diffraction residual stress measurements are nondestructive. Attempts have been made since the 1960's to use nondestructive XRD residual stress measurement for process control, with limited success. The difficulty arises for two fundamental reasons.

First, surface residual stresses simply are not reliably representative of either the processes by which they were produced, or the stresses below the surface (17). Grinding and shot peening will commonly produce nearly identical levels of surface compression. Complete ranges of shot peening intensities will often produce virtually identical surface stresses with large differences in the depth of the compressive layer. Many surface finishing processes like tumbling, wire brushing, sand blasting, etc. will produce nearly identical surface compression which may mask subsurface tensile stresses due to welding, prior grinding, etc. Further, nondestructive surface measurements can not be corrected for potentially large errors due to penetration of the x-ray beam into a stress gradient.

Second, extensive studies have demonstrated that the subsurface peak residual stress rather than the surface residual stress generally governs fatigue life (18). The surface residual stress produced by turning, milling and grinding of steels, nickel, titanium, and aluminum alloys has been found to be the most variable and least characteristic of the machining process. The subsurface peak stress, either tensile or compressive, correlates with both room and elevated temperature fatigue behavior in extensive studies of surface integrity. The subsurface residual stress distribution must generally be obtained to adequately characterize a manufacturing process.

## PROPERTY PREDICTION FROM LINE BROADENING

The breadth of the diffraction peak used for residual stress measurement increases as materials are cold worked, or as a result of phase transformations such as hardening of martensitic steels. The broadening is primarily the result of two related phenomena: a reduction of the "crystallite" or coherent diffracting domain size, and an increase in the range of microstrain. As a material is cold worked, or strained as a result of phase transformations, the perfect crystalline regions between dislocation tangles become smaller. When these regions are reduced to less than nominally  $0.1\mu\text{m}$ , the diffraction peak breadth increases with further reduction. The microstrain in each crystallite will vary about the mean value for the aggregate of such regions making up the polycrystalline body. This range of microstrain results in variation in lattice spacing of the diffracting crystallites, and increased line broadening. Other imperfections such as stacking faults and point defects also contribute to the peak breadth.

The relative contributions of crystallite size and microstrain to the integral breadth can be separated by the Warren-Averbach method (19). However, the separation is of little practical use in engineering applications, requires extensive data collection, and is subject to variations in interpretation. The measured peak breadth, even without correction for instrumental broadening, can be related directly to material properties of practical engineering interest such as the alteration of yield strength in cold worked alloys, and hardness in martensitic steels.

The hardness in martensitic steels can be measured simultaneously with residual stress with depth resolution on the order of the  $5\mu\text{m}$  penetration depth of the x-ray beam. The high depth resolution allows detection of thin work softened layers produced by deformation at the surface of critical components such as gears and bearings. An empirical relationship between the (211) peak breadth and

Rockwell C hardness for SAE 1552 steel is shown in Figure 3 (16). The hardness calculated from peak broadening is compared to mechanical microhardness measurements at an adjacent location on an induction hardened gear tooth in Figure 4. The high resolution of the x-ray diffraction technique allows a clear definition of the hardness gradient through the case-core interface.

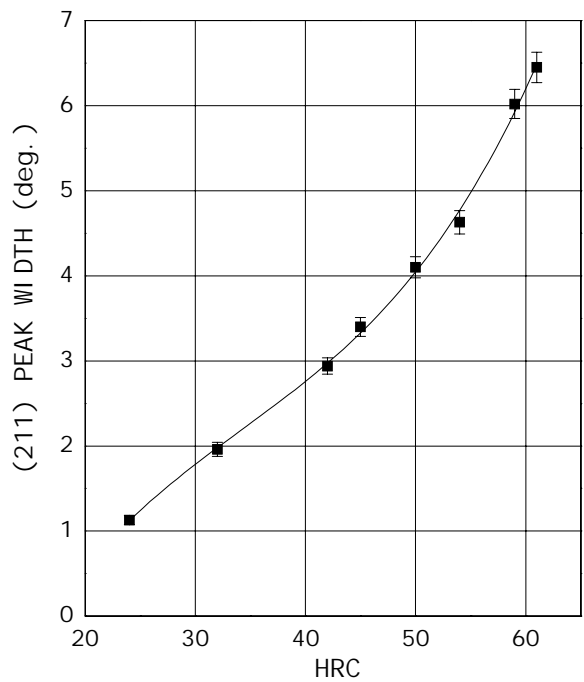
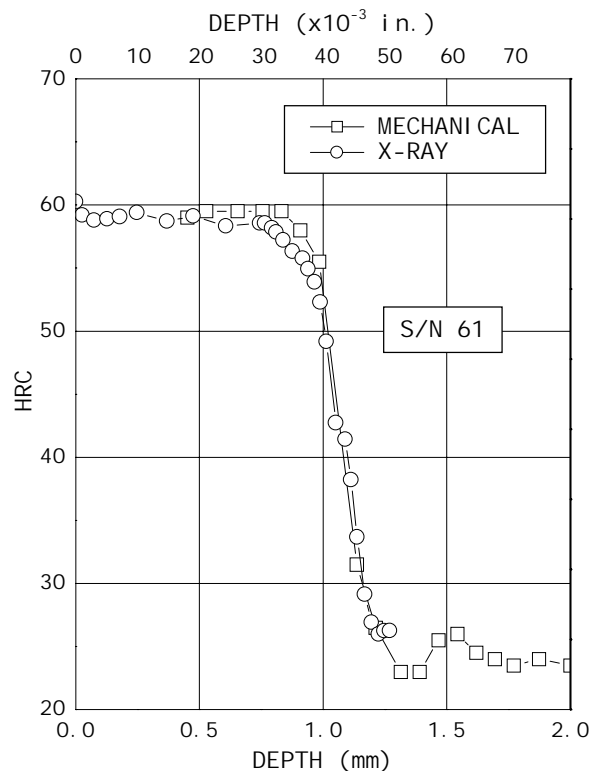


Fig. 3 - Dependence of (211) peak half-width on hardness for



SAE 1552 steel. Data points are an average of five measurements using  $\text{CrK}\alpha$ , peak at  $2\theta = 156\text{ deg}$ . Ref. (16)

Fig. 4 - Comparison of mechanical (Vickers 500g) and XRD hardness measured at adjacent locations on an induction hardened SAE 1552 steel gear tooth. Ref. (16)

The degree to which materials have been cold worked can be estimated from the peak breadth. If "cold work" is defined as the true plastic strain, a true stress-strain curve can then be used to estimate the resulting change in yield strength (20,21). An example of the relationship between the (420) diffraction peak width and the percent cold work (true plastic strain) for the nickel-base super alloy Rene 95 is shown in Figure 5. The results indicate the accumulated peak breadth is independent of the mode of deformation, and is additive for combined deformation, provided true plastic strain is taken as the measure of cold working.

The complex distribution of yield strength developed by weld shrinkage in previously reamed Inconel 600 sleeve is shown in Figure 6 (22). The line broadening data, converted to percent cold work and then yield strength, reveal a complex layer of highly cold worked surface material extending to a depth of 0.25mm in the reamed area adjacent to the heat affected zone. The plastic deformation caused by weld shrinkage extends 25mm to either side of the weld. The material is only fully annealed well beneath the reamed surface in the heat affected zone. Stress corrosion cracks were associated with peak tensile stresses occurring just at the edge of the highly cold worked reamed area. Note that the yield strength of the deformed surface layers after cold working exceeds twice bulk yield of the alloy.

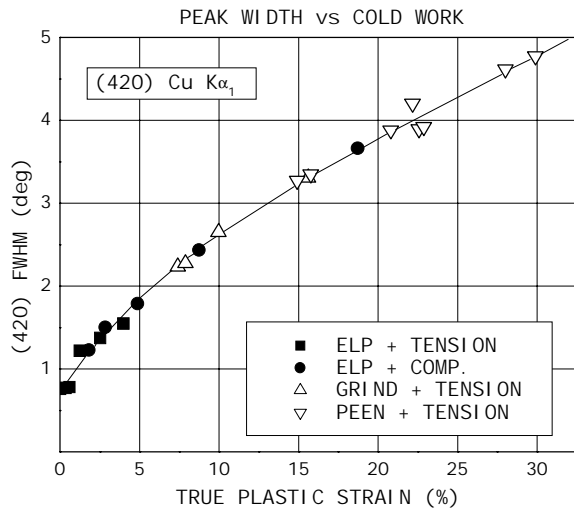


**Fig. 5** - Dependence of the (420)  $K\alpha_1$  peak width on cold work (true plastic strain) showing independence of the mode of deformation and accumulation. Ref. (20)

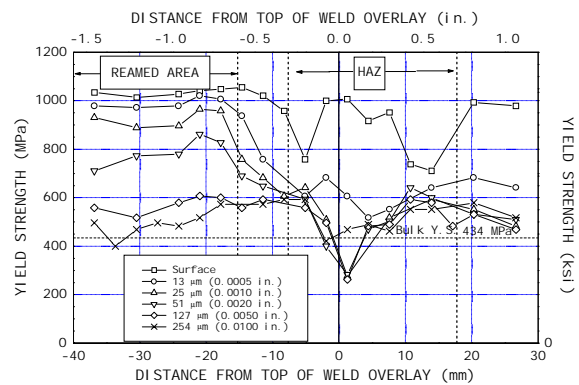


**Fig. 6** - Yield strength distribution calculated from peak breadth on the inside surface of Inconel 600 offer reaming and welding (see text). Ref. (22)

## MODELING OF RESIDUAL STRESS RELAXATION

The relaxation of residual stress during cyclic loading or at elevated temperature has been reported for decades, and has been reviewed (23). Recently, O. Vöhringer and coworkers (24,25) have developed models for the prediction of residual stress relaxation as functions of time and temperature, single cycle overload, and cyclic loading which promise to be powerful tools for failure analysis.

An Avrami approach is used to describe the fraction of residual stress remaining as a function of time and temperature in terms of an activation energy and to other material constants. The material dependent constants are developed from measurements of the isothermal stress relaxation as functions of time. The predicted and measured stress relaxation at the surface of shot peened AISI 4140 steel, using an incremental relaxation approach, is shown in Figure 7. The thermal relaxation model promises prediction of the retention of compressive residual stresses from shot peening in high temperature applications such as high performance gearing and turbine engine components for both failure analysis and design.

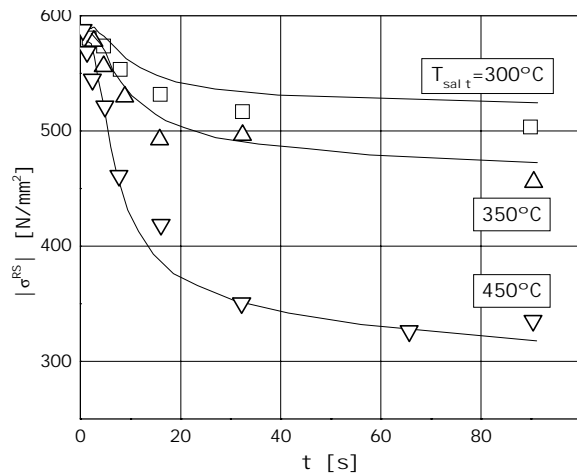


**Fig. 7** - Measured residual macro-stress after short time annealing in salt baths of different temperatures and relaxation curves modeled using the numerical stress-transient method based on an Avrami approach. Ref. (25)

Momentary overload is commonly observed to upset and alter the state of residual stresses. Vöhringer has developed a model allowing prediction of the change in residual stress at the surface of a component as a result of plastic deformation. The residual stress and yield strength of the material in the current state and in each layer beneath the surface is incorporated into a finite element model allowing prediction of changes in surface residual stress. An example showing the change in the surface axial residual stress on 4140 shot peened steel in different heat treatments is shown in Figure 8. The model allows prediction of residual stress redistribution by subsequent deformation as in split-sleeve cold-expansion of reamed holes, overload of turbine disk bores at high RPM, and compressive overloading of shot peened components.

Cyclic loading causes residual stress relaxation for alternating stresses significantly above the endurance limit. Vöhringer has proposed a model describing the fraction of the initial residual stress remaining on the surface of a part exposed to cyclic loading as a linear function of  $\log N$ , where the slope and intercept can be described by material dependent constants, which depend upon the stress amplitude. The model has been applied to both fully reversed bending and axial loading fatigue. The relaxation of surface axial residual stress in shot peened 4140 steel as a function of cycles is shown in Figure 9. After redistribution of stress on initial loading, the surface stress follows a linear reduction with  $\log N$ , until near failure.

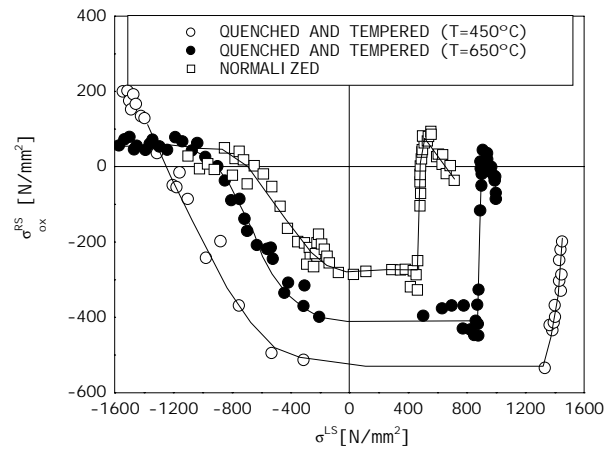


**Fig. 8** - Axial macro-residual stress in differently heat treated and shot peened samples as a function of the quasi-static loading stress. Ref. (25)

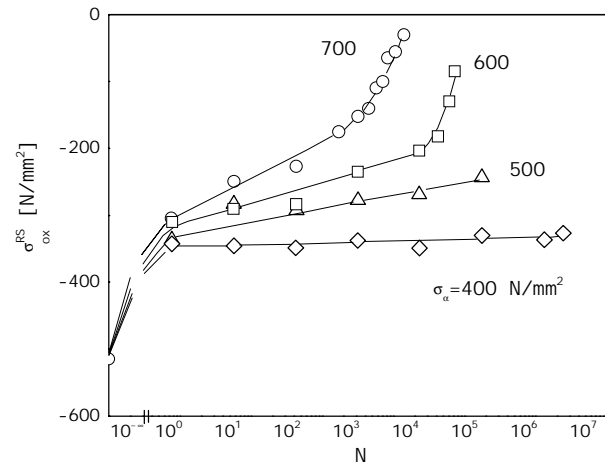


**Fig. 9** - Axial macro-residual stress of quenched and tempered samples as a function of the number of loading cycles for various applied stress amplitudes. Ref. (25)

In failure analysis, the surface residual stress could be compared to areas of the specimen which were in a comparable state of residual stress prior to cyclic loading in order to estimate either the effective cyclic load or the number of cycles of exposure, if the other is known. Applications include prediction of relaxation of residual stresses under known cyclic loading in design and failure analysis.

## CONCLUSIONS

A brief theoretical development and discussion of sources of error shows that the plane-stress model of x-ray diffraction residual stress measurement is the practical approach for engineering applications such as failure analysis and process development. Nondestructive surface residual stress measurements are inadequate for most applications because of errors inherent in uncorrected surface measurements, lack of correlation between surface stresses and the processes which produce them, and the need to know the subsurface peak residual stress to determine the effect on fatigue life.

The diffraction peak width obtained during residual stress measurement can be used to predict material properties such as hardness, percent cold work, and yield strength with high spatial and depth resolution. Current applications include detection of surface deformation producing softening of steels, measuring case depth with stress in induction hardening and increases in yield strength of machined surfaces of work hardenable alloys.

Recent developments in the prediction of residual stress relaxation using x-ray diffraction data have been successfully applied to predict thermal, cyclic, and single cycle upset relaxation of shot peened steels, and promise to become increasingly important tools in design, failure analysis, and process development studies.

## REFERENCES

- 1 Koistinen, D.P. and R.E. Marburger, *Trans. ASM*, 51, 537 (1959).
- 2 Ogilvey, R.E., M.S. Thesis, MIT, 1952.
- 3 Hilley, M.E., ed., "Residual Stress Measurement by X-Ray Diffraction," SAE J784a, 21-24, Soc. of Auto. Engrs. (1971).
- 4 ASTM E837 "Standard Test Method for Determining Residual Stresses by the Hole-Drilling Strain-Gage Method," 1994.
- 5 Cullity, B.D., *Elements of X-ray Diffraction*, 2nd ed., pp 447-76, Addison-Wesley, Reading, Massachusetts (1978)
- 6 Prevéy, P. S., *Adv. X-Ray Anal.*, 20, 345 (1977)
- 7 Dölle, H. and Cohen, J.B., *Met. Trans.*, IIA, 159 (1980).
- 8 Dölle, H., *J. Appl. Cryst.*, 12, 498 (1979).
- 9 Prevéy, P.S. and Mason, P.W., *Practical Applications of Residual Stress Technology*, ed. C. Ruud, pp 77-81, Am. Soc. for Met., Materials Park, Ohio (1991).
- 10 Ruud, C.O. and K. Kozaczek, *Proceedings of the 1994 SEM Spring Conference and Exhibits*, pp 8-13, Soc. for Exp. Mechanics, Bethel, Connecticut (1994)
- 11 Noyan, I.C. and J.B. Cohen, "Residual Stress: Measurement by Diffraction and Interpretation," Springer-Verlag, New York, New York (1987).
- 12 Prevéy, P.S., *Adv. X-Ray Anal.*, 29, 103-111 (1986)
- 13 Gupta, S.K. and Cullity, B.D., *Adv. X-Ray Anal.*, 23, 333 (1980).
- 14 Prevéy, P.S. "Metals Handbook: Ninth Edition," Vol. 10, ed. K. Mills, pp 380-392, Am. Soc. for Met., Metals Park, Ohio (1986).
- 15 Moore, M.G. and Evans, W.P., *Trans. SAE*, 66, 340 (1958)
- 16 Hornbach, D.J., Prevéy, P.S. and Mason, P.W., "X-Ray Diffraction Characterization of the Residual Stress and Hardness Distributions in Induction Hardened Gears," *Proceedings First International Conference on Induction Hardened Gears and Critical Components*, Gear Research Institute, (1995), pp. 69-76.
- 17 Prevéy, P.S., *Practical Applications of Residual Stress Technology*, ed. C. Ruud, pp 47-54, Am. Soc. for Met., Materials Park, Ohio (1991).
- 18 Koster, W.P., et al. "Surface Integrity of Machined Structural Components", AFML-TR-70-11, Air Force Materials Laboratory, WPAFB (1970).
- 19 Warren, B.E. and Averbach, B.L., *J. of Appl. Phys.*, 23, 497 (1952).
- 20 Prevéy, P.S., *Residual Stress in Design, Process and Materials Selection*, ed. W.B. Young, pp 11-19, Am. Soc. for Met., Metals Park, Ohio (1987).
- 21 Prevéy, P.S., *Workshop Proceedings: U-Bend Tube Cracking in Steam Generators*, pp 12-3 to 12-19, Electric Power Research Institute, Palo Alto, California (1981)
- 22 Prevéy, P.S., P.W., Mason, D.J., Hornbach, and Molkenthin, J.P., "Effect of Prior Machining Deformation on the Development of Tensile Residual Stresses in Weld Fabricated Nuclear Components," *Journal of Materials Engineering and Performance*, vol. 5(1), Materials Park, OH, ASM International, 1996 pp. 51-56.
- 23 James, M.R., "Residual Stress and Stress Relaxation," E.Kula and V.Weiss, ed., pp 349-65, Plenum, New York, New York (1985).
- 24 Vöhringer, O., "Residual Stresses," E. Macherauch & V. Hauk, ed., pp 47-80, DGM Informationsgesellschaft-Verlag, Oberursel (1986).
- 25 B. Eigenmann, V. Schulze and O. Vöhringer, *Proc. Int. Conf. on Residual Stress, ICRS IV*, 598-607, SEM, (1994).